Taylor & Francis
Taylor & Francis Group

Ships and Offshore Structures

ISSN: (Print) (Online) Journal homepage: www.tandfonline.com/journals/tsos20

Modelling of a cargo oil pump turbine system to find the optimum pump operation capacities through the design of experiments approaches

Onur Yuksel

To cite this article: Onur Yuksel (21 May 2024): Modelling of a cargo oil pump turbine system to find the optimum pump operation capacities through the design of experiments approaches, Ships and Offshore Structures, DOI: 10.1080/17445302.2024.2336679

To link to this article: https://doi.org/10.1080/17445302.2024.2336679

Published online: 21 May 2024.

SHIPS AND OFFSHORE STRUCTURES
https://doi.org/10.1080/17445302.2024.2336679

Taylor & Francis
Taylor & Francis Group

Modelling of a cargo oil pump turbine system to find the optimum pump operation capacities through the design of experiments approaches

Onur Yuksel

Maritime Faculty, Marine Engineering Department, Zonguldak Bulent Ecevit University, Zonguldak, Turkey

ABSTRACT

This study aims to thoroughly understand and analyze the Cargo Oil Pump Turbine (COPT) system on tanker ships through thermodynamic and numerical simulations. The goal is to find the best pump capacities to match different cargo discharge rates and properties. A parametric study has been performed on the COPT system by building a thermodynamic model including exergy analysis, and a numerical centrifugal pump model. The design of experiment applications which are factorial design and response surface methodology (RSM) have determined the the optimal pump capacity The findings demonstrate that the risky flow rate region for the cavitation, if the density and vapour pressure are close to limits, is between 3050-3500 m^3/h. The factorial design finds the best operating flow rate for the high capacity demands at 4025 m^3/h where the efficiencies are the highest, and the RSM calculates the optimum capacity for the low demands at 1460.34 m^3/h.

ARTICLE HISTORY
Received 6 August 2023
Accepted 11 March 2024

KEYWORDS
Cargo oil pump turbine (COPT); thermodynamic modelling; exergy analysis; factorial design; response surface methodology

1. Introduction

The regulations and applications in the maritime sector have highly focused on the energy efficiency issue to reduce fuel consumption and resulting greenhouse gases (GHG) due to marine operations (Hüffmeier and Johanson 2021). International Maritime Organization (IMO) has put new measures like the Ship Energy Efficiency Management Plan, Energy Efficiency Existing Index (EEXI), and Carbon Intensity Indicator (CII) into effect to reduce the environmental impact sourced from marine vessels (Uyanık et al. 2020; Ivanova 2021; Bayraktar and Yuksel 2023). The production of electricity on marine vessels has been a significant contributor to air pollution because it is a continuous source of emissions. Especially during cargo discharge operations in ports, ship electrical needs are very high, resulting in the release of a remarkable amount of GHG (Styhre et al. 2017). Additionally, the utilisation of marine oil-fired boilers for cargo heating and running steam-driven cargo handling equipment in port operations has also been a great emission producer for tanker vessels (Yuksel and Koseoglu 2022; Yuksel 2023). Enhancing the efficiency of ship equipment, and optimising the marine operations reduce auxiliary machine utilisation with lower fuel consumption which leads to ease of compliance with the IMO requirements on energy efficiency (Bayraktar 2023; Bayraktar et al. 2023). To comply with the updated emission reduction goals set by IMO, the reduction of the auxiliary equipment's fuel usage becomes a critical issue (Konur et al. 2022a).

Oil tankers carry most of the crude oil produced all around the Globe, and the transfer of the crude oil on the tanker vessel is carried out with cargo oil or cargo transfer systems (Vidmar and Perkovič 2018). These systems are responsible for the cargo discharging operations, and their performance majorly affects the staying time of the ship in the terminal (Wang et al. 2021). Therefore, the efficient operation of these systems becomes a crucial issue (Yüksel and Köseoğlu 2020). To successfully discharge the cargo oil from the ship to the tanker terminal, large tanker ships are favourably equipped with steam-powered cargo oil pump turbines (COPTs), which have a relatively high power demand. Large amounts of steam are used to meet the power demand of COPTs, and this steam is returned and cooled so that it can be used in a vacuum condenser's closed circuit once more (Konur et al. 2022b). Although COPTs have a high initial installation cost, they are very dependable and considerably shorten port stays for oil tankers compared to other options (Konur et al. 2022a). Increased cargo transfer speeds are needed and desired by port authorities and ship owners since oil tankers are anticipated to spend fewer hours in ports. Additionally, it is important to think about the safety of the crew as well as the environment during a cargo transfer operation. To meet the mentioned requirements, dependable cargo transfer pumps are essential thus the efficient running of the cargo handling pumps carried out near the best efficiency points during most of the discharge operations yields a faster and more reliable cargo handling process (Sakar and Zorba 2013; Yüksel and Köseoğlu 2020). In addition to reliable operation, the number of boilers should be reduced, when steam-driven cargo pumps are used for the cargo handling to enhance the environmental benefits and energy efficiency of the vessel. Well-planned operation and optimised usage of COPT systems are beneficial and necessary implementations for tanker ships to reduce the fuel consumption of both marine diesel generators and oil-fired boilers (IMO 2013).

Validated thermodynamic or numerical models of engineering systems provide a practical and effective way to investigate the efficiency of systems and detect the optimal operating conditions (Yuksel et al. 2019; Liu et al. 2022). In this regard, researchers have built mathematical models of ship cargo transfer systems or processes and analysed various aspects of the system. Banaszek (2008) investigated the impact of the cargo properties on the hydraulic-driven cargo pump's discharge rate on chemical tankers.

CONTACT Onur Yuksel onur.yuksel@beun.edu.tr Zonguldak Bülent Ecevit University, Marine Engineering, Maritime Faculty, Kepez District, Hacı Eyüp Street, No:1 67300, Kdz. Ereğli/Zonguldak, Türkiye

The pump model was built and validated using the freshwater, then cargoes with different densities and viscosities were analysed. The results indicated that the density has a prominent impact on the discharge rate, on the other the effect of viscosity is lower. Yang et al. (2013) built a cargo pump model inside the LNG handling simulator covering only discharge operations. They highlighted that the simulator could be a significant asset in training utilisation. The completed version of the simulation was presented in the study conducted by Cao and Zou (2014). Kang and Kang (2014) analysed the impact of the flat tank bottom on the cavitation characteristics of a cargo pump through a computational fluid dynamics simulation. An increment of 4.8% on the required net positive suction head ($NPSH_R$) is calculated. The effects of various liquid cargo properties on the performance of the hydraulic-driven cargo transfer pump were analysed by Yüksel and Köseoğlu (2020) through a MATLAB/Simulink pump simulation and Artificial Neural Networks. The findings demonstrated that the performance prediction is performed with satisfactory accuracy and the cargo density has a significant impact on the pump performance and head parameters. Özkan et al. (2023) performed a simulation model-based analysis to minimise the cargo transfer by utilising various pipeline pathways. The outcomes of the study depicted that reducing the waiting time is ensured most effectively by opening a separate line.

Apart from cargo transfer systems or process modelling, studies related to COPT have also been analysed in different ways. Konur et al. (2022b) evaluated the waste heat potential of the COPT system for the utilisation on an organic Rankine Cycle (ORC). The topic was also evaluated comprehensively by Konur et al. (2022a) which is a review study covering marine ORC systems. An automation methodology based on the Internet of Things for a hydraulic-driven submerged cargo pump's purge operation was presented by Kumar and Devi (2021) and the possible challenges and advantages were discussed. Wang et al. (2021) evaluated the operational safety of cargo oil systems on tankers and determined the possible low-performance equipment. Findings depicted that the wear and inadequate lubrication of couplings, journals, universal joints and mechanical seals are the primary causes of the decline in the working performance of cargo oil pumps. Wang et al. (2019) assessed the performance conditions of the components of cargo oil transfer systems. The outcomes demonstrated that the methodology could show how well the cargo transfer system is functioning and serve as a foundation for modifying the loading and unloading activities, which helps to avoid significant failures.

The findings of the literature review illustrate that the studies related to the cargo handling systems of tanker vessels primarily focus on the modelling of and analysis of the system or process, waste heat potential of COPT, automation and condition monitoring of the system. The studies performing numerical modelling concentrate on hydraulic-driven cargo pumps and terminal-based simulations. There has been a literature gap detected about the numerical and thermodynamic modelling and the detecting optimum operating points of COPT pumps. The motivation of the study is to differentiate with comprehensive modelling and analysis of the COPT system. The innovation of the presented numeric modelling methodology is the integration of the turbine and COPT pump model, and the examination of thermodynamic and exergy performance by considering the interaction of the performance changes due to the handling of different fuels having various densities in the COPT pump. The paper also creates novelty by determining the best efficiency points of the COPT system by applying a DOE approach. Highlighting the best efficiency points of the system can contribute to the literature in terms of energy efficiency, safety and possible waste heat applications. The increased awareness of efficient cargo handling can reduce the cargo handling timing which can lead to environmental and economic benefits. The study employs a parametric study on the centrifugal pump side that investigates cavitation characteristics and performance changes with varying cargo properties. In addition, by modelling the Rankine Cycle, the efficiency of the turbine and cycle is investigated. Considering the steam mass flow rate, the boiler fuel consumption is included in the analysis. The optimal operating point ensuring the best performance is determined by using the design of experiments (DOE) approaches.

2. Method

The COPT data have been gathered from an oceangoing crude oil tanker having 149,999 deadweight tonnages. By utilising the collected data, a thermodynamic model of the Rankine cycle including exergy analyses has been formed and analysed parametrically regarding varying mass flow rates of the steam. The fuel consumption of the boiler has also been calculated in this step. Then, the centrifugal pump side of the COPT system has been modelled and the effect of changing cargo properties and flow rate on the discharge/suction pressures, efficiencies and acquired net positive suction head. The pump model has been constructed and validated by using freshwater like the shop test results of the investigated pump given in the ship trial records. Finally, the best efficiency point of the system has been detected using the factorial design and response surface methodology (RSM) approaches, which is one of the DOE methods. The optimum operating point has been determined considering the fuel consumption of the boiler, the thermal efficiency of the system and the centrifugal pump efficiency. Figure 1 illustrates the flowchart of the employed methodology in the paper.

The methods used in the paper are explained with two sub-sections which are system description and modelling. In the system description, the COPT system has been introduced and the specifications of the data used in the model have been explained. In the modelling section, the mathematical background of the methodology has been demonstrated.

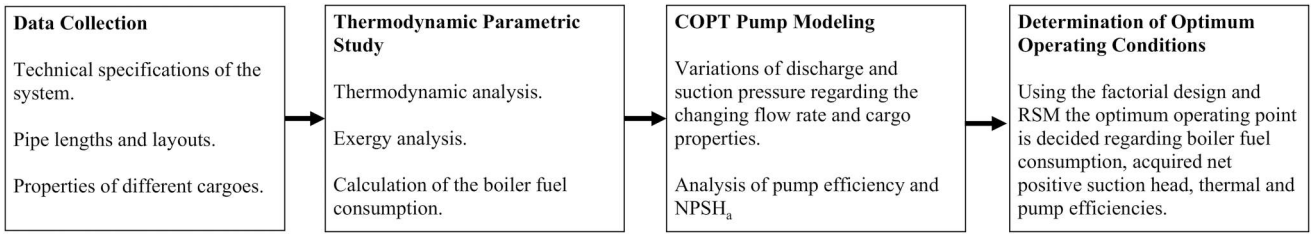

Figure 1. Flowchart of the method used in the paper.

2.1. System description

The COPT system includes two sections which are a turbine, and a cargo pump side. The turbine side produces the work to drive the COPT pump (McGeorge 1995). A vapour cycle named the Rankine Cycle is used to rotate the turbine by utilising the superheated steam produced in the boiler. In the cycle, water enters the pump as a saturated liquid and is compressed. The temperature and pressure of the water are increased in state 2 which becomes a compressed liquid. The boiler is essentially a heat exchanger where heat from combustion gases is transferred to the compressed water and it becomes the superheated vapour because of the heat addition (Kavasoğulları and Cihan 2015). At state 3, superheated steam is entered into the turbine and expanded. Due to the expansion, the work is produced to rotate the shaft of the COPT pump, and the pressure and temperature of the steam drop and enter the condenser. Steam is often a high-quality saturated liquid–vapour mixture at state 4 (Çengel and Bole 2015; Kavasoğulları and Cihan 2015). In the condenser, which is essentially a heat exchanger, steam is condensed at constant pressure by rejecting heat to a cooling medium which is low-temperature cooling water on board (Konur et al. 2020). The cycle is completed when saturated liquid water exits the condenser and enters the pump (Çengel and Bole 2015). Figure 2 illustrates the working principle of the COPT system and mentioned states.

The COPT system is used to transfer crude or product oil in large tankers (Wang et al. 2021). Cargo discharge operations are generally carried out without the main engine working so, the heat addition is conducted by oil-fired boilers on board (Yuksel and Koseoglu 2023). The collected data of the system contain information about the turbine, centrifugal COPT pump, and various crude oil handled in the ship. Table 1 illustrates the general data used in the parametric calculations.

The data described in the table have been obtained from an oceangoing crude oil tanker. The flow rate-dependent data are shop test results of the COPT system provided by the manufacturer during the ship trial tests. The performance experiments conducted on the system have been ensured while feed pumps transfer the water at 36.4°C. Therefore, the validation of the model has been performed using the same fluid as well. Cargo properties have been taken from the cargo records of the vessel. These specifications are recorded by using the documents provided by the authority during cargo loading and the report of a trustworthy laboratory on the cargo samples collected during the operation. The effect of the density variations of the transferred fluid is analysed that's why the principal selection criterion of the cargo is density. The other criterion is the vapour pressure since the cavitation of the COPT pump is wanted to be evaluated through changing flow rate and cargo type. The COPT steam mass flow rate has been adjusted by using a bypass valve 2 located between the boiler and COPT system shown in figure. The pipe lengths, coefficients related to line components, and heights have been gathered from the watch-keeping engineers on board.

2.2. Modelling

The analysis and determination of the most optimum operating conditions of the COPT system have been conducted by thermodynamic modelling, exergy analysis, centrifugal COPT pump modelling and full-factorial design processes. In this section, the mathematical background and logic of these methods have been presented.

There have been limitations to performing the modelling and analysis processes that can be listed as follows:

- The thermodynamic and numeric models covered the steady-state calculations, the sudden peaks and potential small deviations were neglected.
- The pipe lengths and suction-discharge heights were obtained from the duty engineers with the approximate values.
- Similarly, the number of line components, their types, and their properties were gathered from the information given by the duty engineers.

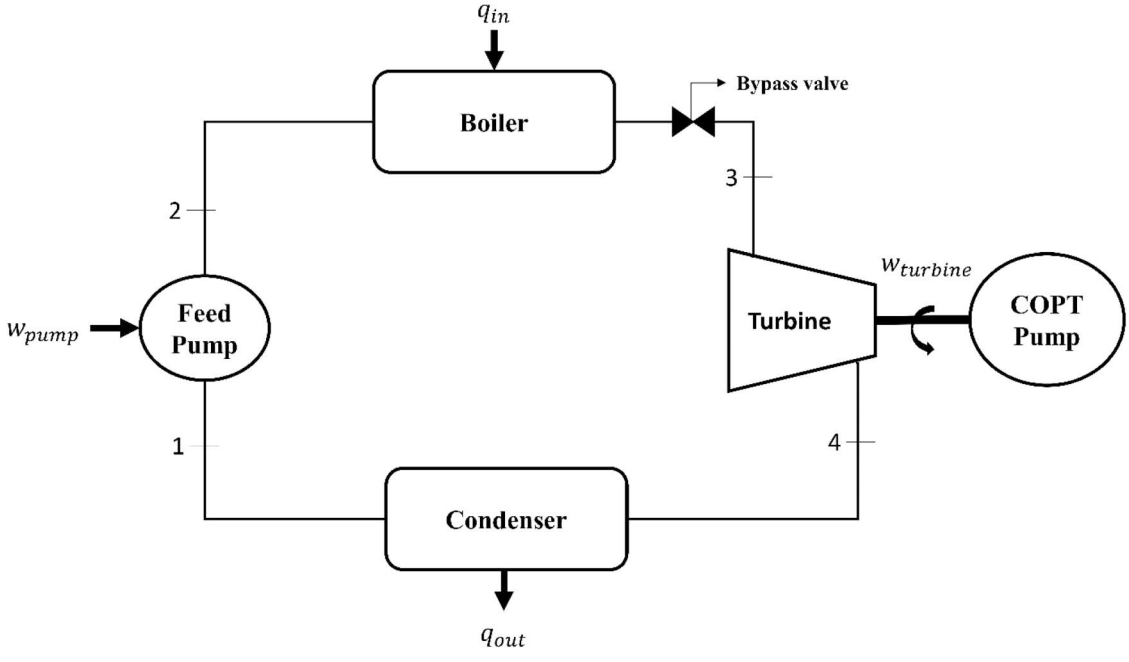

Figure 2. COPT system layout (Çengel and Bole 2015; Kavasoğulları and Cihan 2015).

Table 1. COPT system data used in the model.

Turbine Data				
	Steam Inlet		Exhaust Steam	
COPT Speed (rpm)	Pressure (kPa)	Temperature (°C)	Pressure (kPa)	Steam mass flow rate (kg/s)
680.00	1745.584	256.900	71.9939	3.1011
801.59	1745.584	254.700	72.1272	3.4003
958.63	1716.164	254.800	72.2605	3.7867
1115.00	1735.777	259.2000	72.3939	4.1714
1126.03	1725.970	256.113	72.2605	4.2778
1130.00	1728.568	255.000	72.2958	4.3161

COPT Pump Data		
Parameter	Value	Unit
Suction Bore (D_s)	0.6	m
Discharge Bore (D_d)	0.45	m
Suction Height (z_s)	1	m
Discharge Height (z_d)	10	m
Suction Pipe Length (L_s)	17.753	m
Discharge Pipe Length (L_d)	130	m
Suction Minor Losses Coefficient (K_s)	0.71	–
Discharge Minor Losses Coefficient (K_d)	1.09	–

Capacity (Q) (m^3/h)	Delivery Head (H_d) (m)	Suction Head (H_s) (m)	Velocity Head (H_v) (m)
1050	153	−0.8	0.1
1933	147.5	−2.4	0.4
3035	138.5	−5	1
4025	129	−5	1.7
4170.5498	127.8974	−5	1.847
4223	127.5	−5	1.9

Cargo Properties			
Fuel Name	Density (ρ) (kg/m^3)	Kinematic viscosity (ν) (m^2/s)	Vapour Pressure (P_{vp}) (kPa)
Attaka	810.7	0.000001687	45.5054
Qatar Marine	847.1	0.000009221	35.1633
Iranian Heavy	873.6	0.000025800	41.3685
Eocene	943.1	0.000537000	96.5266

2.2.1. Thermodynamic modelling and exergy analysis

The calculation of the feed pump work (w_{pump}) is ensured by employing Equation (1) (Çengel and Bole 2015; Konur et al. 2020).

$$w_{pump} = V*(P_1 - P_2) \tag{1}$$

where V is the specific volume at state 1, P_1 is the pressure at the feed pump entrance, P_2 is the pressure at the feed pump exit. The specific enthalpy at the feed pump exit (h_2) is calculated by summing the specific enthalpy at the feed pump entrance (h_1) and w_{pump} (Çengel and Bole 2015; Özdemir and Kılıç 2017). The specific enthalpy after the heat addition (h_3) is found from the steam tables and the calculation of the specific enthalpy after the expansion (h_4) requires computing of dryness fraction of the steam (x) shown in Equation (2) (Konur et al. 2020).

$$x = \frac{(s_4 - s_f)}{s_{fg}} \tag{2}$$

where s_4 and s_f are the entropy of the gas and fluid phases. It is assumed that $s_3 = s_4$ and the entropy of state 3 which is found in the steam tables (Holmgren 2006). The specific entropy change of vaporisation (s_{fg}) is also detected from the tables. The added heat in the boiler (q_{in}), the rejected heat through the condenser (q_{out}), the work output of the cycle (w_{net}) and thermal efficiency (η_{the}) are calculated by employing Equations (3)–(6) (Yazıcı and Selbaş 2011; Çengel and Bole 2015).

$$q_{in} = h_3 - h_2 \tag{3}$$

$$q_{out} = h_4 - h_1 \tag{4}$$

$$w_{net} = q_{in} - q_{out} \tag{5}$$

$$\eta_{the} = w_{net}/q_{in} \tag{6}$$

The net turbine power transmitted to the COPT pump ($\dot{W}_{net}$) is computed by multiplying w_{net} to steam mass flow rate ($\dot{m}_{steam}$) and turbine efficiency (η_{turb}). The formula is demonstrated in Equation (7) (Özdemir and Kılıç 2017; Konur et al. 2020).

$$\dot{W}_{net} = w_{net}*\dot{m}_{steam}*\eta_{turb} \tag{7}$$

The exergy analysis of the system has been performed considering processes 1–2 and 3–4 are isentropic ($s_1 = s_2$, $s_3 = s_4$) that does not involve irreversibility. Internally reversible processes are assumed as 2–3 and 4–1 which are constant-pressure heat addition and heat rejection, respectively (Moran et al. 2010; Çengel and Bole 2015). The exergy destruction of the process 2–3 ($X_{dest,2-3}$) has been calculated by employing Equation (8), while Equation (9) depicts the exergy destruction formula of the process 4–1 ($X_{dest,4-1}$) (Moran et al. 2010; Çengel and Bole 2015; Özdemir and Kılıç 2017; Yuksel et al. 2019).

$$X_{dest,2-3} = T_0*(s_3 - s_2 - \frac{q_{in}}{T_H}) \tag{8}$$

$$X_{dest,4-1} = T_0*(s_4 - s_1 - \frac{q_{out}}{T_0}) \tag{9}$$

where T_0 is the temperature of the surroundings where heat is rejected, T_H is the temperature of the steam in the boiler taken as 515°C (Behrendt and Szczepanek 2022). The exergy destruction of the cycle ($X_{dest,cycle}$) is found by addition of $X_{dest,2-3}$ and $X_{dest,4-1}$. Expended exergy ($X_{expended}$) is calculated by employing Equation (10) (Moran et al. 2010; Çengel and Bole 2015), and Equation (11) computes the second law efficiency (η_{II}) of the cycle (Yazıcı and Selbaş 2011; Çengel and Bole 2015).

$$X_{expended} = q_{in}*\left(1 - \frac{T_0}{T_H}\right) + w_{pump} \tag{10}$$

$$\eta_{II} = 1 - \frac{X_{dest,cycle}}{X_{expanded}} \tag{11}$$

2.2.2. Boiler fuel consumption

Equation (12) is utilised to calculate the fuel consumption of the boiler ($\dot{m}_{fuel}$) in kg/s (Miura 2008; Yuksel 2023).

$$\dot{m}_{fuel} = \frac{\dot{m}_{steam}*q_{in}}{\eta_{boiler}*LCV_{fuel}} \tag{12}$$

where η_{boiler} is the efficiency of the boiler assumed at 0.85 (Miura 2008), LCV_{fuel} is the lower calorific value of the heavy fuel oil which is 40,200 kJ/kg (IMO 2016).

2.2.3. Centrifugal COPT pump model

The system manometric height or head (H) can be calculated by employing Equations (13)–(17) (Bachus and Custodio 2003; Yüksel and Köseoğlu 2020).

$$H = H_{st} + H_p + H_v + H_L \tag{13}$$

$$H_{st} = z_d - z_s \tag{14}$$

$$H_p = \frac{P_d - P_s}{\rho g} \tag{15}$$

$$H_v = \frac{v_d^2 - v_s^2}{2g} \tag{16}$$

$$H_L = H_f + H_m = \left(f_d \frac{L_d}{D_d} + \sum\nolimits_d^K\right)\frac{v_d^2}{2g} + \left(f_s \frac{L_s}{D_s} + \sum\nolimits_s^K\right)\frac{v_s^2}{2g} \tag{17}$$

where H_{st} is the static head, H_p represents pressure head, the velocity head is denoted by H_v, and H_L is the total pipe and pipe components' losses. Static height of suction and discharge sides are expressed as z_s and z_d, the velocities in the suction and discharge lines are denoted as v_s and v_d. L_s and L_d are pipe lengths of suction and discharge sides, D_s and D_d represent bores of suction and discharge pipes. Friction coefficients of two sides are denoted by f_s and f_d, the coefficients to compute minor losses (H_m) are depicted by K_s and K_d presented in Table 1. The density of the handled fluid is represented by the ρ. The friction losses (H_f) are calculated by utilising the Darcy–Weisbach formula shown in Equation (17). The calculation of the friction coefficient (f) for suction and discharge lines is conducted by employing the Colebrook Equation demonstrated in Equation (18) when the Reynolds Number (Re) is higher than 4000 (Bachus and Custodio 2003; Demirel and Er 2008).

$$f = \frac{0.25}{\log\left(\frac{k}{3.7D} + \frac{3.74}{Re^{0.9}}\right)^2} \tag{18}$$

where k is the mean roughness of the pipe's inner surface and D is the pipe diameter indicated for suction and discharge sides as D_s and D_d in Table 1. The efficiency of the COPT pump is computed by utilising Equation (19) (Bachus and Custodio 2003).

$$\eta_{pump} = \frac{\rho g H Q}{1000 \dot{W}_{net}} \tag{19}$$

where Q is the volumetric flow rate of the COPT pump. To evaluate the cavitation of the COPT pump the acquired net positive suction head ($NPSHH_A$) is calculated by employing Equation (20) (Green 2019; Yüksel and Köseoğlu 2020).

$$NPSH_A = \frac{P_s}{\rho g} - \frac{P_{vp}}{\rho g} + + z_s - H_f \tag{20}$$

where P_{vp} is the vapour pressure of the handled fluid. The $NPSH_A$ must be at least 0.6 m more than the required net positive suction head ($NPSH_R$) calculated by using Equation (21) (Green 2019).

$$NPSH_R = \left(\frac{n\sqrt{Q_{opt}}}{S_q}\right)^{4/3} \tag{21}$$

where n is the revolution per minute of the COPT pump, Q_{opt} is the optimum volumetric flow rate of the COPT pump (4025 m^3/h) provided by the manufacturer, and S_q is the suction-specific speed taken as 800 (Demirel and Er 2008; Green 2019).

2.2.4. Full factorial design

To find the optimum operating flow rates of the COPT pump, full factorial design experiments have been conducted by utilising Minitab Software which is widely employed in many different fields. Users of this software can undertake statistical analysis using its capabilities, which include DOE, regression analysis, hypothesis testing and analysis of variance (Minitab 2023). The variables for the experiment that the researcher controls are referred to as factors (Rakić et al. 2014). Factors can be independent in the sense that their levels do not depend on one another. However, there is a chance that two or more variables will interact, meaning that the impact on one variable's reaction will rely on the other variables' value (Buragohain and Mahanta 2008). The selected factors are $\dot{m}_{fuel}$, η_{pump} and η_{the} with six levels regarding changing flow rate and cavitation limits.

All levels of each element in an experiment are coupled with all levels of every other factor in a factorial design (Kechagias et al. 2020). The experimental strategy entails making observations for every potential combination that can result from the various amounts of the components and a treatment combination is any unique combination (Buragohain and Mahanta 2008). The most typical factorial design has two levels and n factors, or a 2^n factorial design. Consider a 2-level, n-factor system. Experiment data must be chosen to be at each of the n-dimensional space's corners. The data in a 2^3-factorial design should therefore be chosen so that they are located at each corner of a three-dimensional hypercube (Buragohain and Mahanta 2008; Kechagias et al. 2020). It takes eight experiments plus central point replications to complete the 2^3 full factorial designs and the mathematical model of the experiment is depicted in Equation (22) (Rakić et al. 2014).

$$y = b_0 + b_1x_1 + b_2x_2 + b_3x_3 + b_{12}x_1x_2 + b_{13}x_1x_3 + b_{23}x_2x_3 \tag{22}$$

where y represents the response, b_i indicates linear terms and b_{ij} denotes interaction terms. The determination of the success of satisfying the objectives is ensured regarding individual and composite desirability terms. Composite desirability (CD) assesses how the circumstances optimally maximise a collection of replies, while individual desirability (d) assesses how the conditions optimally optimise a single response. Desirability is measured on a scale from 0 to 1. Zero signifies that one or more responses fall outside of the permissible range, whereas one represents the optimum situation. The importance of reaching the goal value can be emphasised or diminished by choosing a weight between 0.1 and 10. The target and the bounds are given equal weight when the weight is set to 1. This environment is referred to as neutral and applied in the study (Minitab 2023).

2.2.5. Response surface methodology

To find the optimal operating capacity at low load demands $NPSH_A$ is added to the model as an additional response. RSM is performed in Minitab Software considering Q as the continuous factor on $NPSH_A$, $\dot{m}_{fuel}$, η_{pump} and η_{the}. The addition of the target of maximising $NPSH_A$ forces the model to look up lower capacity regions which is the main purpose of the RSM utilisation. The RSM is a group of statistical and mathematical methods for developing empirical models. A response (output variable) that is impacted by several independent variables (x_i) is to be optimised through proper experiment design. To determine the causes of variations in the output response, a series of tests known as runs are used as an experiment (Khuri and Mukhopadhyay 2010). Equation (23) is

the main formula for the first-degree RSM model.

$$y = b_0 + \sum_{i=1}^{k} b_i x_i + e \tag{23}$$

where e is the error rate. The RSM model is used to identify the x parameters that produce the maximum (or minimum) response over a certain region of interest.

3. Results and discussion

The validation of thermodynamic and centrifugal COPT pump models, the findings and comments of the parametric study run on these models, and full factorial design experiments have been demonstrated in this section. The waste heat potential of the system and outcomes related to the operational efficiency of the system have also been indicated. The Rankine cycle has been modelled with some assumptions, and turbine efficiency is calculated at 0.728 which is close to the given 0.75 value in the manufacturer's datasheet. The thermodynamic model calculates a 2.93% error rate compared to test data which is at acceptable limits considering the assumptions presented in the modelling section. The validity of the centrifugal pump has been evaluated by comparing the system head given in the test results and the calculated system head shown in Figure 3.

In Figure 3 the model calculations fit the test data with the mean absolute error at 0.01152 and mean absolute percentage error at 0.00805% which indicates a satisfactory validation performance of the centrifugal COPT pump model. Figure 4 illustrates the variation of steam mass entering the turbine and COPT pump discharge volumetric flow rates regarding the $\dot{W}_{net}$.

The amount of steam entering the turbine is less affected by the $\dot{W}_{net}$ than the capacity of the COPT pump. This inference is useful in interpreting the boiler fuel consumption and understanding the optimum operating points. Figure 5 shows the energy and exergy efficiencies of the system regarding COPT pump flow rate change. The remaining parameters calculated in the analyses are demonstrated in Table 2.

Figure 3 depicts that the best efficiency points are obtained at the COPT pump capacity of 4025 m^3/h also detected as the Q_{opt} by the manufacturer. The η_{the} and η_{II} are also high at the lowest flow rate which can be evaluated for the low load conditions during the cargo transfer operations. The details of the results of the parametric thermal and exergy analyses are in Table 2. The steam inlet temperature

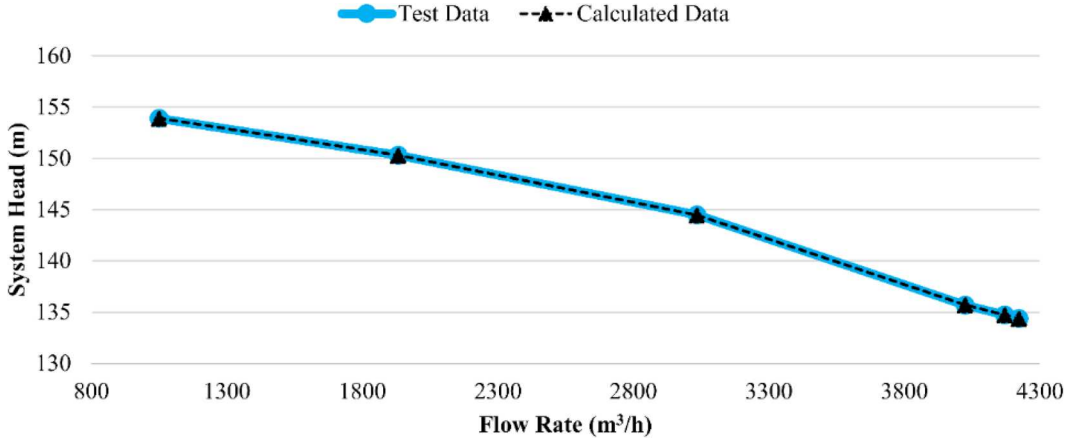

Figure 3. The benchmarking between the test and calculated system head.

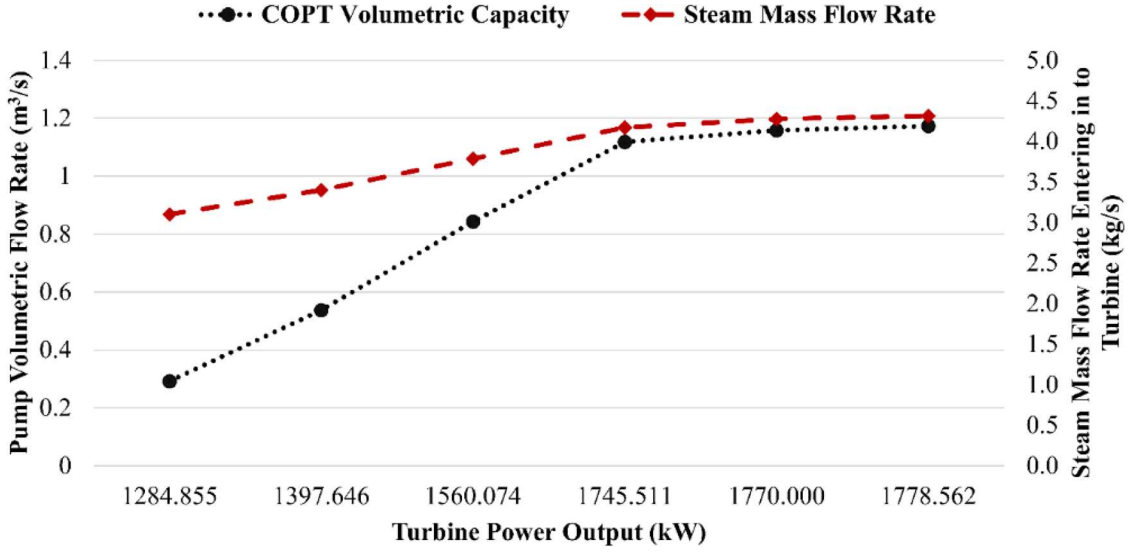

Figure 4. The variation of the flow rates regarding the turbine power output.

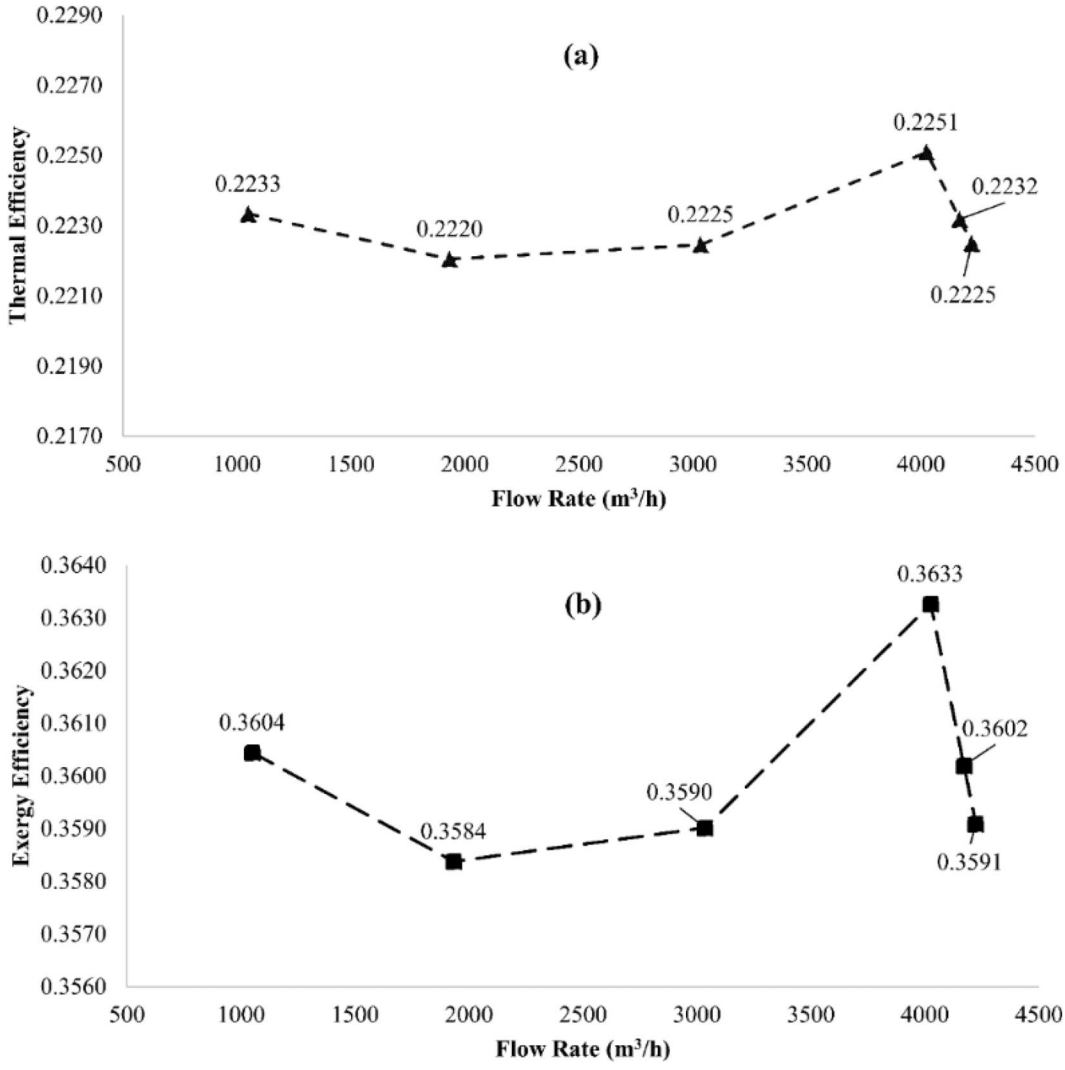

Figure 5. Energy (a) and exergy (b) efficiencies of the system regarding the COPT pump capacity.

Table 2. Results of the exergy and energy analysis of the system.

Q	$X_{dest,2-3}$	$X_{dest,4-1}$	$X_{dest,cycle}$	$X_{expended}$	q_{in}	q_{out}	w_{net}	$\dot{W}_{net,iso}$
1050	664.1422	349.1406	1013.283	1584.355	2549.274	1979.936	569.3375	1765.579
1933	663.0597	351.2903	1014.35	1580.912	2543.729	1978.901	564.8278	1920.571
3035	665.4179	348.3889	1013.807	1581.647	2544.962	1978.825	566.1365	2143.77
4025	665.6823	345.2329	1010.915	1587.649	2554.597	1979.587	575.0095	2398.588
4170.55	664.7029	349.0426	1013.745	1581.711	2545.049	1978.797	566.2518	2444.006
4223	664.9674	348.0282	1012.996	1583.288	2547.584	1979.008	568.5755	2432.24

in the analysis has varied between 527.7 and 532.2 K depending on the steam mass flow rate. The waste heat potential can be expressed by using the q_{out} which is an average of 1979.176 kJ/kg for the cycle. The mean $X_{expended}$ is calculated at 664.6621 kJ/kg and the average $X_{dest,cycle}$ is found as 1013.0887. Figure 6 indicates $\dot{m}_{fuel}$ in t/h regarding the increasing capacity of the COPT pump.

The fuel consumption of the boiler increases linearly until the Q reaches 4225 m^3/h which is the maximum allowable capacity of the COPT pump. The COPT pump model has been run with cargoes having various densities and vapour pressures depicted in Table 1, and the impacts of the changing fluid properties and flow rate on the pressure, η_{pump} and $NPSH_A$ have been observed. Figure 7 illustrates the change of suction and discharge pressures with the increasing flow rate and varying cargo properties.

The suction pressure shown in Figure 7(a) increases when the density of the fluid decreases. With water, which is the densest fluid, the suction pressure is −0.1694 bars when the COPT pump capacity is 1050 m^3/h. When the flow rate increases the suction pressure drops −0.5347 bars until 3050 m^3/h and after this point, a slight increase is calculated. For the least dense cargo the suction pressure is found −0.1383 bars at the flow rate of 1050 m^3/h, and −0.4363 bars at the COPT pump capacity of 3050 m^3/h. The discharge pressures decrease with the increasing flow rates and decreasing density. When the COPT pump handles the water, the discharge pressure starts from 13.846 bars and decreases to 9.9652 bars as the flow rate increases. The reduction of the density leads to lower discharge pressures as expected. Figure 8 indicates the COPT pump efficiency change when the pump handles different cargoes at changing flow rates.

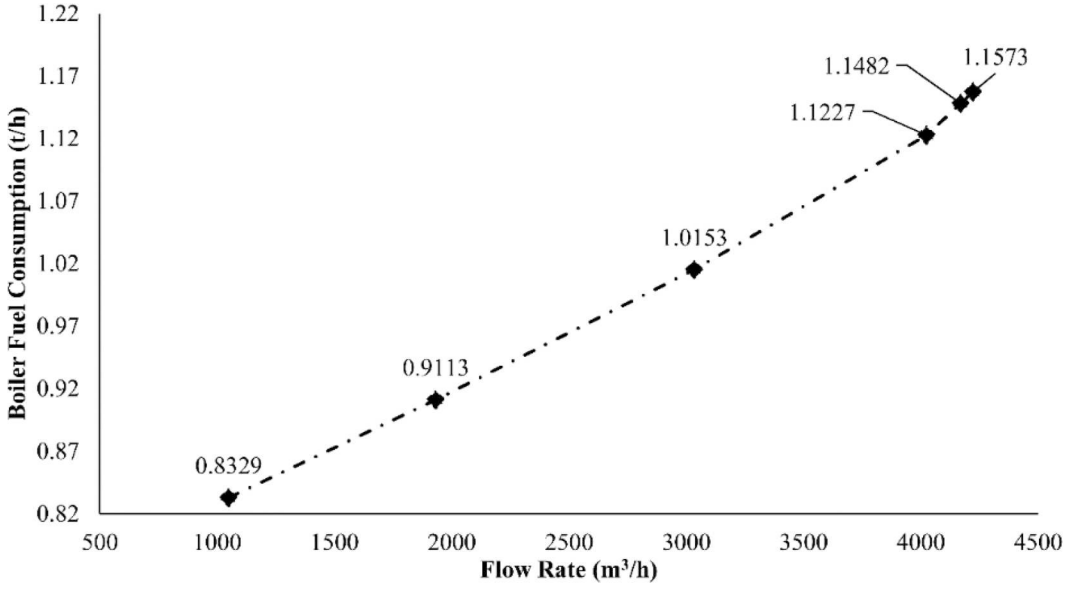

Figure 6. The boiler fuel consumption with varying flow rates of the COPT pump.

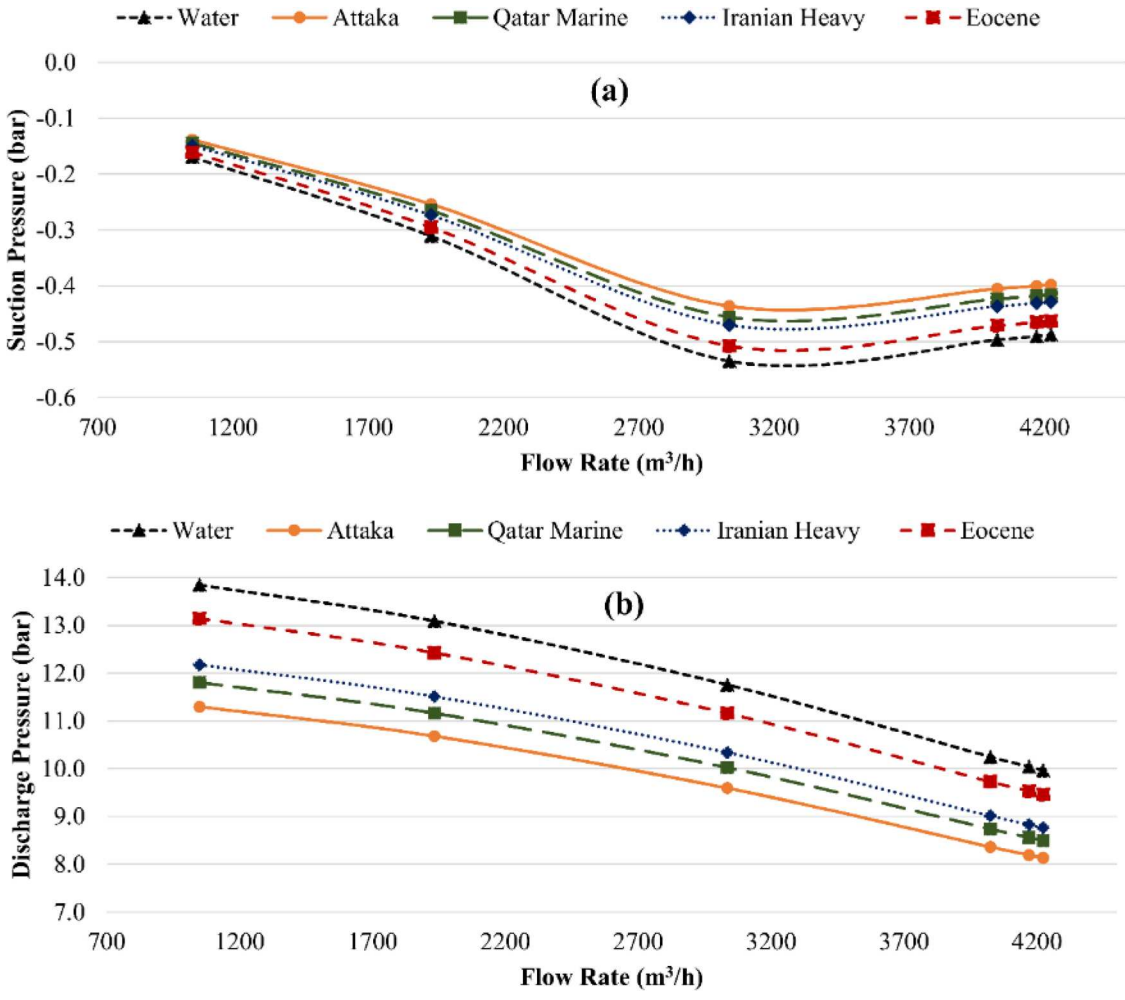

Figure 7. The pressure changes regarding the cargo type and flow rate at the suction (a) and discharge (b) sides.

The capacity and higher density of the handled fluid yield an increment in the pump efficiency observed in Figure 8. The highest efficiency at the maximum capacity is achieved at 0.864 for the water and the lowest is 0.705 for the Attaka at the same capacity. Figure 9 illustrates the changes of $NPSH_A$ regarding varying density and flow rates.

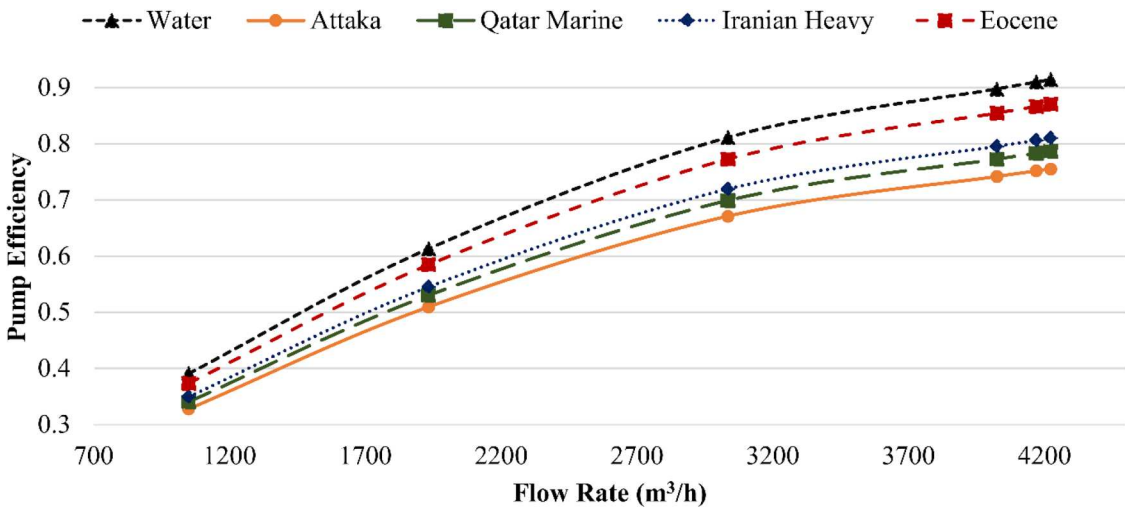

Figure 8. The change in pump efficiency regarding the cargo type and flow rate.

$NPSH_R$ is found at 1.73 m for the COPT pumps and the limit for $NPSH_A$ becomes 2.33 m shown in Figure 9. When the fluid density is reduced the $NPSH_A$ tends to decrease and the increment of the vapour pressure impacts negatively the $NPSH_A$. While the pump handles Attaka and Iranian Heavy cargoes, the $NPSH_A$ remains under the limit which indicates a risk of cavitation at the pump discharge capacities are between 3050 and 3500 m^3/h. This capacity range results in the lowest $NPSH_A$ for all evaluated fluids. Table 3 indicates a ranking of the most suitable operating discharge capacities of the COPT pump regarding the selection provided by the factorial design approach. The DOE has been performed on the water dataset since the trends are found similar when other fluids are handled in the model.

The CD is the highest for the Q at 4025 m^3/h which is an expected selection since it is the optimum flow rate point of the pump. At the 4025 m^3/h capacity the η_{the} is achieved at the highest value, and η_{pump} is also at a satisfactory level. The second solution is at the COPT pump capacity where the cavitation risk for some cargo types starts. This solution offers a relatively lower $\dot{m}_{fuel}$ while η_{the} and η_{pump} is at lower conditions compared to the first solution. The CD value decreases sharply for the third solution which provides moderate η_{the} and higher $\dot{m}_{fuel}$ with an increased η_{pump}. The CD value is the poorest for the capacity of 1933 m^3/h which can offer a lower $\dot{m}_{fuel}$ and be suitable for the low-capacity demands of the terminal. Figure 10 illustrates the fitting line of the first solution detected by the factorial design approach with d values for each factor.

In Figure 10, the η_{the} is achieved at the highest value which yields the value is 1, and similarly η_{pump} is at near maximum value with a d value of 0.9679. The d value for the $\dot{m}_{fuel}$ remains relatively low at 0.1067 and reduces the CD significantly, however, this solution highlights the importance of the utilisation at the optimum flow rate when the capacity demand from the terminal is at a high level. The usage of the one-step further can reduce operational efficiency remarkably. In addition, the solutions have been focused on meeting high and moderate capacity demands but sometimes the operation needs to be performed at low flow rates. The fourth solution provides a very low CD that requires looking for alternative combinations. The factorial design approach has ensured the ranking of the existing combinations regarding the d and CD successfully. However, the investigation of the intermediate values has become a necessity for low-capacity operations since the existing

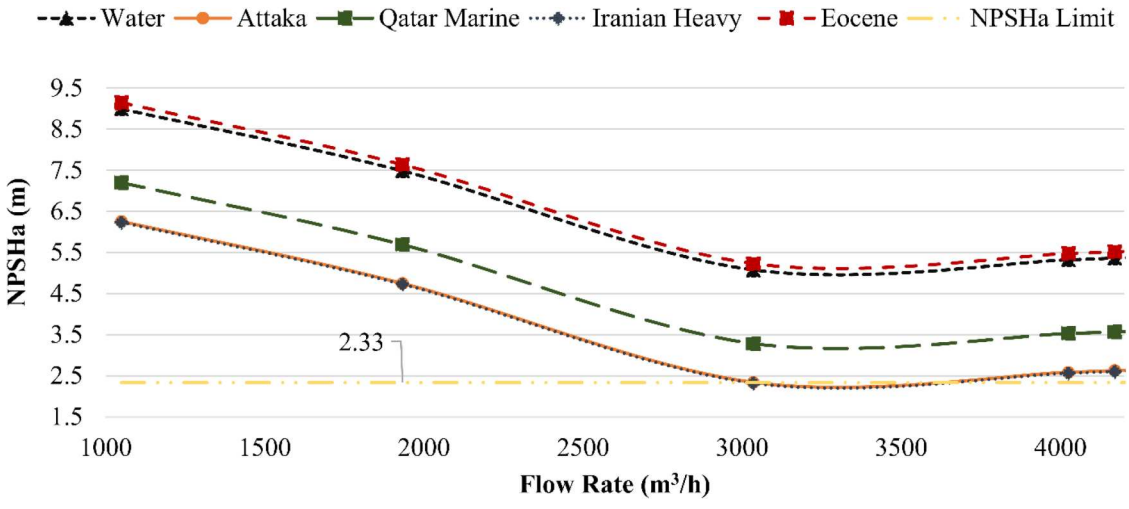

Figure 9. The changes of $NPSH_A$ regarding varying density and flow rates.

Table 3. The solutions of the factorial design approach.

		Fit			
Solution	Q	η_{the}	η_{pump}	$\dot{m}_{fuel}$	CD
1	4025.00	0.22509	0.85	1.16	0.4692
2	3035.00	0.22245	0.76	1.05	0.3610
3	4170.55	0.22249	0.86	1.18	0.1598
4	1933.00	0.22205	0.56	0.94	0.026

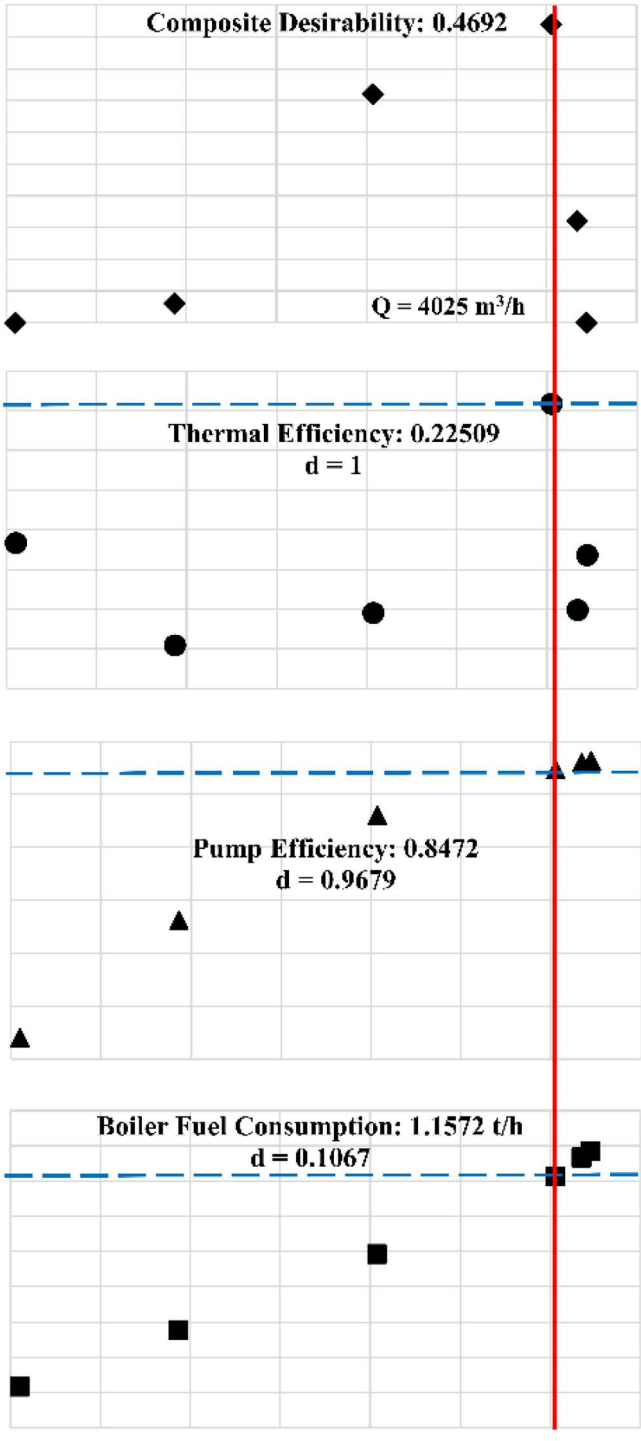

Figure 10. The fitting line of the solution with the highest CD found by the factorial design.

Table 4. The solutions of the RSM approach.

		Fit				
Solution	Q	η_{the}	η_{pump}	$\dot{m}_{fuel}$	$NPSH_A$	CD
1	1460.34	0.2227	0.4519	0.8939	8.068	0.43
2	3704.88	0.2242	0.8194	1.0880	5.2228	0.22

flow rate and factor combinations couldn't provide a solution with a satisfactory CD value. To solve the issue first of all RSM approach has been used and $NPSH_A$ has been added to the factors and its target is set as maximisation which enforces the RSM approach looking for low-capacity regions. Table 4 demonstrates the solutions found by the RSM.

The highest CD is attained for the flow rate of 1460.34 m^3/h with a successful $\dot{m}_{fuel}$ and $NPSH_A$ fits while the efficiencies are kept at medium fits. This solution can be selected as the low-demand operating point that provides low fuel consumption for the boiler. Although the second solution is for higher capacity demand, the selected flow rate is out of the cavitation risk region which can be aimed for medium to high demands from the terminal existing during the cargo discharge operations. Figure 11 illustrates the fitting line of the best solution found by the RSM with d values for each factor.

The d value is the highest for $\dot{m}_{fuel}$ which yields lower boiler fuel consumption during the low load operations. For $NPSH_A$ there is a satisfactory d value on the other hand efficiencies have lower d values which is an expected result since the COPT pump efficiency increases with the rising flow rate, and thermal efficiency is highest at the optimal flow rate. The d values for the efficacies are still acceptable since the optimum flow rate low load operations have been investigated in this analysis.

The thermodynamic and exergy analyses of the system have indicated that the COPT system has a remarkable waste heat depicted as q_{out} which complies with the findings from Konur et al. (2022b). By utilising an organic Rankine cycle-based waste heat recovery system (WHRS) having 14.29% (Konur et al. 2023), the COPT system can alone provide an average specific energy output of 282.8243 kJ/kg. Depending on the mass flow rate and size of the system, a considerable amount of power output can be obtained during cargo operations. The WHRS applications are mainly built by utilising the main engine exhaust waste heat, and the functionality of the system depends on the operation of the main engine. In other words, the WHRS is not working during the port and harbour operations if the waste heat sources are selected based on the main engine. The mentioned waste heat potential of the COPT system can keep the WHRS in operation and the power generated from WHRS to ship electricity generation plant reduces the number or load of working generators which leads to lower fuel consumption during port and terminal operations (Peralta et al. 2019; Korkmaz et al. 2023).

The selection of the optimum COPT pump capacity is another crucial issue in terms of safety (Wang et al. 2021), and effective operation (Wang et al. 2019). The steam production in the terminal operations has been conducted by the oil-fired boilers which are one of the air pollutants during port operations. Ensuring the minimum fuel consumption sourced by the auxiliary machinery can be beneficial both environmentally and economically (Fan et al. 2021). The DOE approaches have detected the optimal operating flow rate of the COPT pump for meeting both low and high-capacity demands. Aiming the suggested flow rates during the operation yields a more efficient utilisation of the system. The parametric

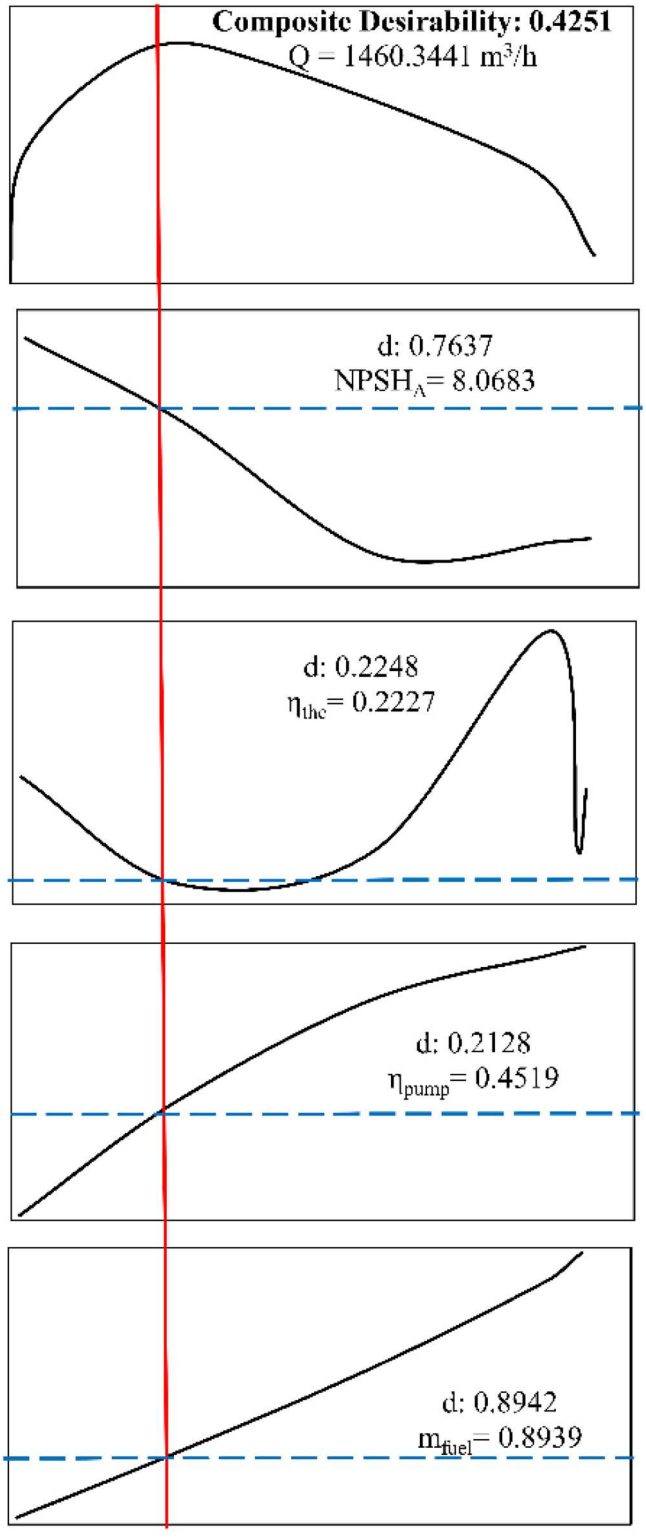

Figure 11. The fitting line of the solution with the highest CD calculated by the RSM.

analyses have demonstrated that the cargo having low densities and high vapour pressures causes the $NPSH_A$ decreasing under the threshold value. This increases the risk of cavitation for specific flow rate regions of the COPT pump. Keeping the flow rate of the COPT pump in the proposed regions helps for avoiding the cavitation risk as well. The long term expression the cavitation reduces the COPT pump performance significantly (Binama et al. 2016; Gu et al. 2022) which prevents energy-efficient operation (Medvitz et al. 2002).

4. Conclusion

The thermodynamic modelling of the Rankine cycle and the numerical simulation of the centrifugal pump side of the COPT system were ensured in the study. The energy and exergy analyses were performed to determine the waste heat potential and the destroyed energy during the cycle. The parametric evaluations were conducted by varying the flow rate of the COPT pump and cargo properties to assess the efficiency of the system. By utilising the factorial design and RSM approaches, the optimum operating capacities of the COPT pump have been investigated. The factorial design was built by considering $\dot{m}_{fuel}$, η_{pump} and η_{the} are the factors depending on the Q. The model depicted the ranking of the best-fitted solutions in the given data set. To search for the optimum flow rate for low-capacity demands, the RSM approach was utilised and $NPSH_A$ was added to the factors. Its target was assigned to be maximised which ensured that the model was searching for lower flow rate regions. The main conclusions can be driven from the mentioned analyses can be listed as follows:

- Thermal and exergetic efficiencies were obtained highest at the flow rate of 4025 m^3/h.
- The average waste heat potential was calculated at 1979.176 kJ/kg while the average destroyed cycle exergy was found at 1013.0887 kJ/kg.
- The peak boiler fuel consumption was computed at the flow rate of 4025 m^3/h.
- The decrease in the density of the cargo yielded a lower suction and a higher discharge pressure.
- The increase in capacity and density led to higher COPT pump efficiency.
- The increase in vapour pressure and decrease in density caused the reduction in $NPSH_A$ that increased the cavitation risk for some cargoes.
- The flow rate regions covering 3050–3500 m^3/h contained a higher risk of cavitation.
- The factorial design found the optimal flow rates at 4025 and 3050 m^3/h for high and medium capacity demands.
- The RSM calculated the best solution to meet low-capacity demand at 1460.34 m^3/h.

This study can be beneficial for academicians working in a related field, marine engineers, or duty officers who are responsible for the cargo discharge operations onboard. The study contributes to the literature by modelling and performing a parametric analysis of the COPT while determining optimal flow rates for the discharge operation. In future studies, a multi-objective metaheuristic optimisation algorithm can be used to determine the optimal operation points and the results can be benchmarked with the findings with DOE approaches.

Nomenclature

Symbol	*Definition*	*Unit*
b_i	Linear terms in the factorial design and RSM	–
b_{ij}	Interaction terms in the factorial design and RSM	–

(*Continued*)

Continued.

Symbol	Definition	Unit
CD	Composite desirability	–
COPT	Cargo oil pump turbine	–
d	Individual desirability	–
DOE	Design of experiments	–
D	Pipe diameter	m
D_d	Discharge pipe diameter	m
D_s	Suction pipe diameter	m
f	The friction coefficient	–
f_d	The friction coefficient of the discharge line	–
f_s	The friction coefficient of the suction line	–
g	The gravitational acceleration	m^2/s
GHG	Greenhouse gases	–
h_1	Specific enthalpy at the pump entrance (state 1)	kJ/kg
h_2	Specific enthalpy at the pump exit (state 2)	kJ/kg
h_3	Specific enthalpy after the heat addition (state 3)	kJ/kg
h_4	Specific enthalpy after the heat rejection (state 4)	kJ/kg
H	System manometric height	
H_d	Delivery head	m
H_f	Friction losses	m
H_L	The total pipe and pipe components sourced losses	m
H_m	Minor losses	m
H_p	Pressure head	m
H_s	Suction head	
H_{st}	Static height head	m
H_v	Velocity head	m
IMO	International Maritime Organization	–
k	Mean roughness of pipe's inner surface	mm
K_d	The coefficient of minor losses (valve, elbow, etc.) in the discharge line	–
K_s	The coefficient of minor losses (valve, elbow, etc.) in the suction line	–
L_d	The length of the discharge line	m
L_s	The length of the suction line	m
LCV_{fuel}	The lower calorific value of the fuel	kJ/kg
$\dot{m}_{steam}$	The mass flow rate of the steam entering in turbine	kg/s
$\dot{m}_{fuel}$	The mass flow rate of the fuel burnt in the boiler	kg/s – t/h
n	The revolution per minute of the COPT pump	rpm
$NPSH_A$	The acquired net positive suction head	m
$NPSH_R$	The required net positive suction head	m
ORC	Organic Rankine Cycle	–
P_1	Pressure at pump entrance (state 1)	kPa
P_2	Pressure at pump exit (state 2)	kPa
P_{atm}	Atmospheric pressure	Pa
P_d	Pressure at the COPT pump discharge line	Pa
P_s	Pressure at the COPT pump suction line	Pa
P_{vp}	Vapour pressure of the handled fluid	Pa
Q	Volumetric flow rate	m^3/h
q_{in}	The added heat in the boiler	kJ/kg
Q_{opt}	The optimum flow rate of the pump	m^3/h
q_{out}	The rejected heat through the condenser	kJ/kg
Re	Reynolds Number	–
RSM	Response Surface Methodology	–
s_3	Specific entropy of the gas phase (from steam tables at state 3)	kJ/kg.K
s_4	Specific entropy of the gas phase (from steam tables at state 4)	kJ/kg.K
s_f	Specific entropy of the fluid phase (from fluid properties table)	kJ/kg.K
s_{fg}	Specific entropy changes of vaporisation	kJ/kg.K
S_q	Suction specific speed	–
V	Specific volume at state 1	kg/m^3
v_d	The velocity of the fluid in the discharge line	m/s
v_s	The velocity of the fluid in the suction line	m/s
w_{net}	The net-specific work output of the cycle	kJ/kg
$\dot{W}_{net}$	The actual power transmitted to the COPT pump	kW
$\dot{W}_{net,iso}$	The isentropic power of the turbine	kW
w_{pump}	Required pump work in the Rankine Cycle.	kJ/kg
x	The dryness fraction of the steam	–
$X_{dest,2-3}$	Exergy destruction of the process 2–3	kJ/kg
$X_{dest,4-1}$	Exergy destruction of the process 4–1	kJ/kg
$X_{dest,cycle}$	Exergy destruction of the cycle	kJ/kg
$X_{expended}$	The amount of exergy used to heat the steam in the boiler	kJ/kg

(*Continued*)

Continued.

Symbol	Definition	Unit
x_i	The independent variables in the factorial design and RSM	
y	The response in the factorial design	–
z_d	The height at that pump discharges the fluid	m
z_s	The height at that the pump sucks the fluid	m
Greek Letters		
η_{boiler}	Boiler efficiency	–
η_{II}	The second law of efficiency	–
η_{the}	Thermal efficiency	–
η_{pump}	The efficiency of the COPT pump.	–
η_{turb}	Turbine efficiency	–
ν	Kinematic viscosity of the handled fluid	m^2/s
ρ	The density of the handled fluid	kg/m^3

Disclosure statement

No potential conflict of interest was reported by the author(s).

Data availability statement

The authors confirm that the data supporting the findings of this study are available within the article [and/or] its supplementary materials.

ORCID

Onur Yuksel http://orcid.org/0000-0002-5728-5866

References

Bachus L, Custodio A. 2003. Know and understand centrifugal pumps. Oxford: Elsevier.

Banaszek A. 2008. The influence of liquid cargo properties on the discharge rate of submerged cargo pumps with hydraulic drive on modern product and chemical tankers. Arch Mech Eng. 55(2):173–191. doi:10.24425/ame.2008.131620.

Bayraktar M. 2023. Investigation of alternative fuelled marine diesel engines and waste heat recovery system utilization on the oil tanker for upcoming regulations and carbon tax. Ocean Eng. 287:115831. doi:10.1016/j.oceaneng.2023.115831.

Bayraktar M, Yuksel O. 2023. A scenario-based assessment of the energy efficiency existing ship index (EEXI) and carbon intensity indicator (CII) regulations. Ocean Eng. 278(April):114295. doi:10.1016/j.oceaneng.2023.114295.

Bayraktar M, Yuksel O, Pamik M. 2023. An evaluation of methanol engine utilization regarding economic and upcoming regulatory requirements for a container ship. Sustain Prod Consum. 39:345–356. doi:10.1016/j.spc.2023.05.029.

Behrendt C, Szczepanek M. 2022. Effect of waste heat utilization on the efficiency of marine main boilers. Energies. 15(23):9203. doi:10.3390/en15239203.

Binama M, Muhirwa A, Bisengimana E. 2016. Cavitation effects in centrifugal pumps – a review. Int J Eng Res Appl. 6(5):52–63.

Buragohain M, Mahanta C. 2008. A novel approach for ANFIS modelling based on full factorial design. Appl Soft Comput. 8(1):609–625. doi:10.1016/j.asoc.2007.03.010.

Cao JH, Zou X. 2014. Analyzing and modeling for liquid cargo handling of LNG simulator. Appl Mech Mater. 668-669:1687–1691. doi:10.4028/www.scientific.net/AMM.668-669.1687.

Çengel Y, Bole M. 2015. Thermodynamics: an engineering approach. 8th ed. Buczek LK, Stenquist B, editors. New York: McGraw Hill.

Demirel K, Er İD. 2008. Gemi mühendisleri için pompa. 1st ed. İstanbul: Birsen Yayınevi.

Fan A, Wang J, He Y, Perčić M, Vladimir N, Yang L. 2021. Decarbonising inland ship power system: alternative solution and assessment method. Energy. 226 (X):120266. doi:10.1016/j.energy.2021.120266.

Green PC. 2019. Predicting centrifugal pump type and NPSH in early facility design. In: Houston: 48th Turbomachinery & 35th Pump Symposia. p. 1–23.

Gu Y, Yu L, Mou J, Shi Z, Yan M, Wu D. 2022. Influence of circular non-smooth structure on cavitation damage characteristics of centrifugal pump. J Brazilian Soc Mech Sci Eng. 44(4):1–21. doi:10.1007/s40430-022-03459-1.

Holmgren M. 2006. X Steam for Matlab [Internet]. [accessed 2023 June 9]. https://studieinfo.liu.se/download/coursedocument/19f7d704-b530-4c15-8a06-0655dec1f6e9/X Steam for Matlab.pdf.
Hüffmeier J, Johanson M. 2021. State-of-the-art methods to improve energy efficiency of ships. J Mar Sci Eng. 9(4):447. [accessed 2023 Jun 1]. doi:10.3390/jmse9040447.
IMO. 2013. Ship-port interface and energy efficiency [Internet]. [accessed 2024 Jan 24]. https://wwwcdn.imo.org/localresources/en/OurWork/Environment/Documents/Air pollution/M5 ship-port interface final.pdf.
IMO. 2016. Amendments to the 2014 guidelines on the method of calculation of the attained energy efficiency design index (EEDI) for new ships (resolution MEPC.245(66), as amended by resolution MEPC.263(68)) [Internet]. [accessed 2023 Jun 9]. https://wwwcdn.imo.org/localresources/en/KnowledgeCentre/IndexofIMOResolutions/MEPCDocuments/MEPC.281(70).pdf.
Ivanova G. 2021. Analysis of the specifics in calculating the index of existing marine energy efficiency EEXI in force since 2023. In: 2021 13th Electr Eng Fac Conf BulEF 2021. doi:10.1109/BulEF53491.2021.9690805.
Kang BY, Kang SH. 2014. Effect of the flat tank bottom on performance and cavitation characteristics of a cargo pump. J Mech Sci Technol. 28(8):3051–3057. doi:10.1007/s12206-014-0712-3.
Kavasoğulları B, Cihan E. 2015. Organik Rankine çevrimi ile birlikte çalışan buhar sıkıştırmalı bir soğutma çevriminin ekserji analizi. Tesisat Mühendisliği Derg. 150(June):74–85.
Kechagias JD, Aslani KE, Fountas NA, Vaxevanidis NM, Manolakos DE. 2020. A comparative investigation of Taguchi and full factorial design for machinability prediction in turning of a titanium alloy. Meas J Int Meas Confed. 151:107213. doi:10.1016/j.measurement.2019.107213.
Khuri AI, Mukhopadhyay S. 2010. Response surface methodology. Wiley Interdiscip Rev Comput Stat. 2(2):128–149. doi:10.1002/wics.73.
Konur O, Colpan CO, Saatcioglu OY. 2022a. A comprehensive review on organic Rankine cycle systems used as waste heat recovery technologies for marine applications. Energy Sources Part A Recovery Util Environ Eff. 44(2):4083–4122. doi:10.1080/15567036.2022.2072981. [Internet]. [accessed 2023 May 31].
Konur O, Saatcioglu OY, Korkmaz SA, Erdogan A, Colpan CO. 2020. Heat exchanger network design of an organic Rankine cycle integrated waste heat recovery system of a marine vessel using pinch point analysis. Int J Energy Res. 44(15):12312–12328. doi:10.1002/er.5212.
Konur O, Yuksel O, Korkmaz SA, Colpan CO, Saatcioglu OY, Muslu I. 2022b. Thermal design and analysis of an organic Rankine cycle system utilizing the main engine and cargo oil pump turbine based waste heats in a large tanker ship. J Cleaner Prod. 368(January):133230. doi:10.1016/j.jclepro.2022.133230.
Konur O, Yuksel O, Korkmaz SA, Ozgur Colpan C, Saatcioglu OY, Koseoglu B. 2023. Operation-dependent exergetic sustainability assessment and environmental analysis on a large tanker ship utilizing organic Rankine cycle system. Energy. 262(PA):125477. doi:10.1016/j.energy.2022.125477.
Korkmaz SA, Erginer KE, Yuksel O, Konur O, Colpan CO. 2023. Environmental and economic analyses of fuel cell and battery-based hybrid systems utilized as auxiliary power units on a chemical tanker vessel. Int J Hydrogen Energy. 48(60):23279–23295. doi:10.1016/j.ijhydene.2023.01.320.
Kumar RP, Devi VA. 2021. Automation of FRAMO cargo pump purging with IoT. In: 21st Annu Gen Assem IAMU AGA 2021 - Proc Int Assoc Marit Univ, IAMU Conf. [place unknown]; p. 444–453.
Liu Y, Yu M, Yu J. 2022. An improved 1-D thermodynamic modeling of small two-phase ejector for performance prediction and design. Appl Therm Eng. 204:118006. doi:10.1016/j.applthermaleng.2021.118006.
McGeorge H. 1995. Marine auxiliary machinery. 7th ed. London: Elsevier.
Medvitz RB, Kunz RF, Boger DA, Lindau JW, Yocum AM, Pauley LL. 2002. Performance analysis of cavitating flow in centrifugal pumps using multiphase CFD. J Fluids Eng. 124(2):377–383. doi:10.1115/1.1457453.
Minitab. 2023. Response optimization [Internet]. [accessed 2023 June 13]. https://support.minitab.com/en-us/minitab/21/help-and-how-to/statistical-modeling/using-fitted-models/supporting-topics/response-optimization.
Miura. 2008. Service News [Internet]; p. 1–3. https://www.miuraz.co.jp/en/marine/pdf/news2.pdf.
Moran MJ, Shapiro HN, Boettner DD, Bailey MB. 2010. Fundamentals of engineering thermodynamics. 7th ed. Ratts L, Dumas S, Kulesa T, Goldstein S, editors. Hoboken (NJ): Wiley.
Özdemir E, Kılıç M. 2017. Energy and exergy analysis of an organic Rankine cycle using different working fluids from waste heat recovery. Uluslararası Çevresel Eğilimler Derg [Internet]. 1(1):32–45. https://dergipark.org.tr/ijent/issue/32841/368720
Özkan ED, Koçer UU, Nas S, İşlek Ö, Tüzgen E, Doğan A. 2023. A simulation model for evaluating the cargo transfer alternatives in liquid cargo terminals. Simulation. 99(1):23–39. doi:10.1177/00375497221107938.
Peralta CPO, Vieira GTT, Meunier S, Vale RJ, Salles MBC, Carmo BS. 2019. Evaluation of the CO 2 emissions reduction potential of Li-ion batteries in ship power systems. Energies. 12(3):375–319. doi:10.3390/en12030375.
Rakić T, Kasagić-Vujanović I, Jovanović M, Jančić-Stojanović B, Ivanović D. 2014. Comparison of full factorial design, central composite design, and Box-Behnken design in chromatographic method development for the determination of fluconazole and its impurities. Anal Lett. 47(8):1334–1347. doi:10.1080/00032719.2013.867503.
Sakar C, Zorba Y. 2013. Operational efficiency at chemical tankers. İstanbul: Beta.
Styhre L, Winnes H, Black J, Lee J, Le-Griffin H. 2017. Greenhouse gas emissions from ships in ports – case studies in four continents. Transp Res Part D Transp Environ. 54:212–224. doi:10.1016/j.trd.2017.04.033.
Uyanık T, Karatuğ Ç, Arslanoğlu Y. 2020. Machine learning approach to ship fuel consumption: A case of container vessel. Transp Res Part D Transp Environ. 84(May):102389. doi:10.1016/j.trd.2020.102389.
Vidmar P, Perkovič M. 2018. Safety assessment of crude oil tankers. Saf Sci. 105:178–191. doi:10.1016/j.ssci.2018.02.009.
Wang C, Fan S, Yao Y, Wu J, Wang B, Zheng L. 2021. Operational safety evaluation of tanker cargo oil system fusing multiple task information. Ocean Eng. 239(September):109856. doi:10.1016/j.oceaneng.2021.109856.
Wang C, Fan SD, Yao YN. 2019. Health status assessment method of oil tanker cargo handling system. In: 2019 Progn Syst Heal Manag Conf PHM-Qingdao 2019. 0:1–6. doi:10.1109/PHM-Qingdao46334.2019.8943004.
Yang ZZ, Zhang XK, Cao JH. 2013. Discharging part of LNG liquid cargo handling simulator. Res J Appl Sci Eng Technol. 6(21):3978–3985. doi:10.19026/rjaset.6.3499.
Yazıcı H, Selbaş R. 2011. Bir Buharli Güç Santralinin Enerji ve Ekserji Analizi. Selçuk Tek Derg. 10(1):117–135.
Yuksel O. 2023. A comprehensive feasibility analysis of dual-fuel engines and solid oxide fuel cells on a tanker ship considering environmental, economic, and regulation aspects. Sustain Prod Consum. 42:106–124. doi:10.1016/j.spc.2023.09.012.
Yuksel O, Gulmez Y, Konur O, Korkmaz SA, Erdogan A, Colpan CO. 2019. Performance assessment of a marine freshwater generator through exergetic optimization. J Clean Prod. 219:326–335. doi:10.1016/j.jclepro.2019.02.083.
Yüksel O, Köseoğlu B. 2020. Modelling and performance prediction of a centrifugal cargo pump on a chemical tanker. J Mar Eng Technol. 19(4):278–290. doi:10.1080/20464177.2019.1665330.
Yuksel O, Koseoglu B. 2022. Regression modelling estimation of marine diesel generator fuel consumption and emissions. Trans Marit Sci. 11(1):79–94. doi:10.7225/toms.v11.n01.w08.
Yuksel O, Koseoglu B. 2023. Numerical simulation of the hybrid ship power distribution system and an analysis of its emission reduction potential. Ships Offsh Struct. 18(1):78–94. doi:10.1080/17445302.2022.2028435.